ADVANCED OPTICAL MATERIALS
www.advopticalmat.de

Cucurbituril-Confined Tetracation Supramolecular 2D Organic Framework for Dual-Emission TS-FRET

*Fan-Fan Li, Man Huo, Jing Kong, and Yu Liu**

Herein, cucurbituril-regulated supramolecular multi-dimensional organic framework constructed is reported by tetraphenylvinyl grafted bromophenylpyridine salt derivatives (TPE-BrN) and cucurbit[n]uril (n = 6, 7, 8) via non-covalent cross-linked, giving supramolecular macrocycle-confined fluorescence-phosphorescence dual emission at 560 and 510 nm in solid state. Different from the formation of TPE-BrN⊂CB[6] complexes and TPE-BrN⊂CB[7] nanoparticle, TPE-BrN⊂CB[8] manifested high-efficient 2D network assembly. TPE-BrN⊂CB[8] assembly can effectively activate triplet-state to singlet-state Förster resonance energy transfer (TS-FRET) with long-lived near-infrared emission at 675 nm via doping organic dye Nile red (NiR) and the energy transfer efficiency reached up to 99%. Although CB[7] can also induce the typical phosphorescence emission at 510 nm, there is no TS-FRET occurring after doping NiR into TPE-BrN⊂CB[7] assembly due to the formation of different assembly modes. The multicolor long-lived emission has been demonstrated very well based on the TS-FRET process activated by CB[8] macrocyclic confined 2D organic framework, which can be successfully applied to fingerprint imaging and the construction of logic gate systems. It provides a novel method for supramolecular macrocycle confined phosphorescence regulation and the development of luminescent materials.

1. Introduction

Supramolecular macrocycle confined induction or extension photoluminescence in particular with pure organic room-temperature phosphorescence (RTP) has become a research hotspot owing to their ultralong lifetime and large stokes shift, which have received enormous attention in bioimaging,[1–3] information encryption and anti-counterfeiting,[4–8] organic light-emitting diodes,[9,10] and so on. Efficient RTP emission[11] can be achieved by suppressing the non-radiative transition of phosphorescent molecules and promoting inter-system crossing (ISC). Many reports have revealed macrocyclic confinement phosphorescence behavior because host-guest interaction[12,13] has been proven to be a fantastic way to acquire highly efficient RTP emission[14–16] in aqueous solution or solid state. Especially, cucurbit[n]urils (CB[n], n = 6, 7, 8) with rigid cavities can suppress molecular vibrations by tightly encapsulating the guest molecules, thereby attenuating the non-radiative transition. For example, George and co-workers reported supramolecular phosphors by host-guest encapsulation between CB[7] and phthalimide derivative in aqueous solution with a remarkable phosphorescence quantum yield.[17] Our group has proposed the macrocyclic-confinement inducing and boosting supramolecular phosphorescence behavior including bromophenylpyridinium salt and its derivatives with CB[n] (n = 6, 7, 8) which showed uncommon RTP emission.[18,19] CB[8] with a large cavity can encapsulate two guests to form a 1:2 stoichiometry supramolecular assembly, which can be utilized to build a multidimensional supramolecular system.

Other than supramolecular 2D organic framework,[20–23] CB[8]-mediated 2D network has been successfully built by forming 2:1 complexes between CB[8] and multi-arm guest molecules via noncovalent interaction to promote photoluminescence properties.[24] Tetracation guests have been well-known as the significant construction block to fabricate highly ordered supramolecular 2D organic framework structure.[25,26] The formation of a 2D network assembly can restrict the free rotation of tetracation guests, resulting in them exhibiting unique photophysical properties in aggregated states. For example, Cao et al. reported a new type of shape-controlled fluorescent supramolecular organic frameworks formed by host-guest interaction between tetraphenylvinyl derivatives and CB[8] in aqueous solution, which served as a stimulus-responsive fluorescent switch that can be applied in cellular imaging.[27,28] Moreover, 2D phosphorescence networks served as a significant luminescent topological morphology, which was expected as a light-harvesting platform to reveal effective triplet-state to singlet-state Förster resonance energy transfer (TS-FRET), thus attaining long-lived luminescent system. However, CB[8] macrocyclic confined fluorescence-phosphorescence dual emission promotes a 2D network activated TS-FRET process, which have not been reported as the best of our knowledge.

In present research (**Scheme 1**), we constructed a purely organic 2D network phosphorescence materials based on tetraphenylvinyl (TPE) derivative and CB[8], which achieved efficient

F.-F. Li, M. Huo, J. Kong, Y. Liu
Department of Chemistry
State Key Laboratory of Elemento-Organic Chemistry
Nankai University
Tianjin 300071, P. R. China
E-mail: yuliu@nankai.edu.cn

The ORCID identification number(s) for the author(s) of this article can be found under https://doi.org/10.1002/adom.202400453

DOI: 10.1002/adom.202400453

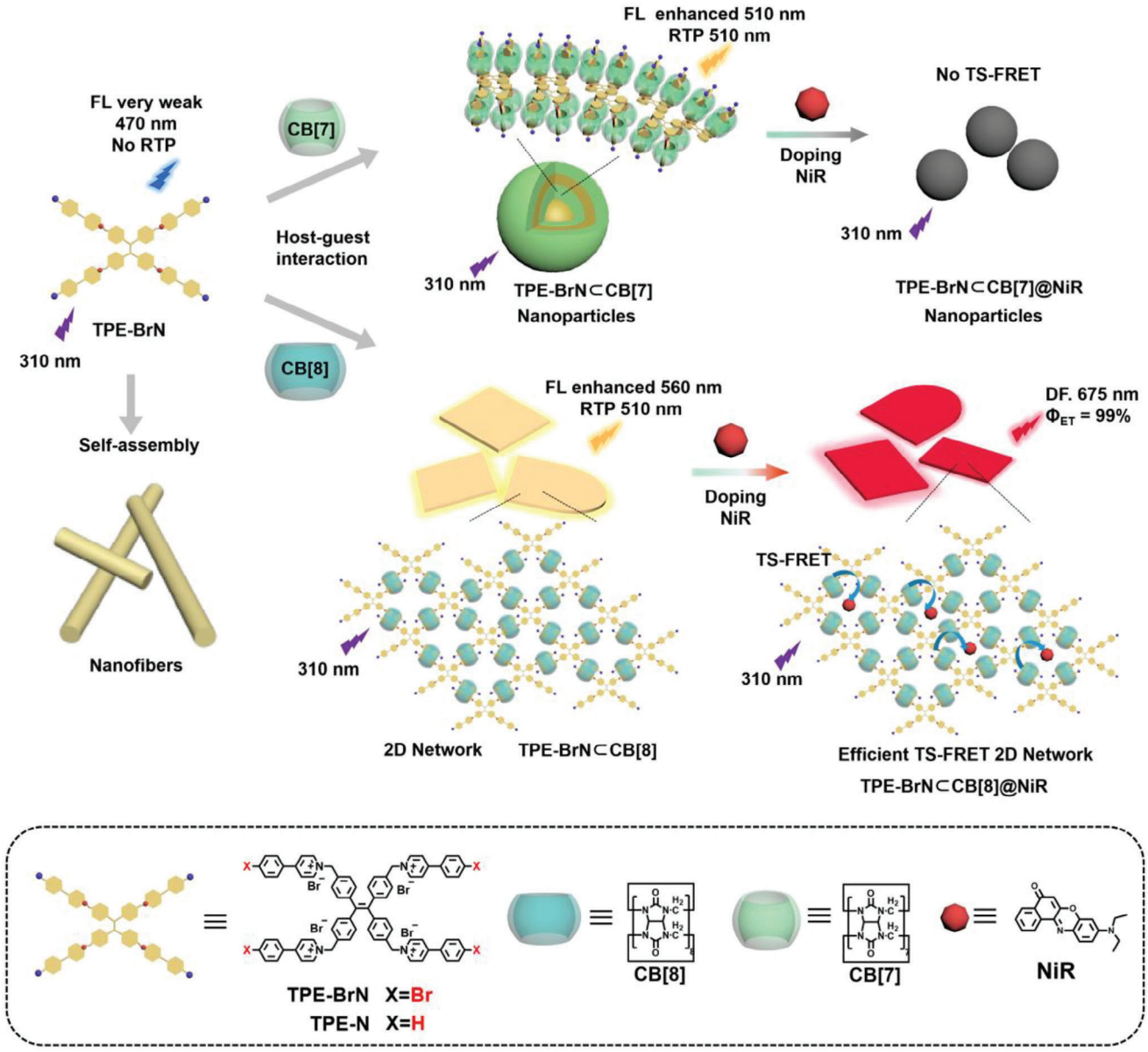

Scheme 1. Construction of solid-state supramolecular 2D network based on cucurbituril confinement for high-efficiency TS-FRET.

TS-FRET process via introducing organic dyes NiR into the supramolecular organic 2D network. CB[n] (n = 6, 7, 8) with cavities of different sizes can induce topological morphology transition from nanofiber to nanoparticle or 2D network which showed various photophysical behaviors. The fluorescence emission of TPE-BrN was centered at 470 nm, and it did not show phosphorescence emission. Subsequently, TPE-BrN was employed as the guest to associate with CB[6], CB[7] and CB[8], leading to the appearance of RTP emission originating from bromophenylpyridine salt and TPE fluorescence emission. Especially, CB[8]-based organic 2D framework would produce large redshift from 470 to 560 nm due to the formation of 2:1 complexes to greatly limit the motion of TPE molecules. In view of the excellent supramolecular 2D topological structure and phosphorescent properties, TPE-BrN⊂CB[8] was utilized to serve as the light-capturing platform. Even though doping trace amounts of NiR (4%) in the TPE-BrN⊂CB[8] 2D network structure as energy acceptor, high-efficiency TS-FRET could be achieved, thus displaying long-lived solid emission. Eventually, this material was applied to latent fingerprint imaging and logic gates, which has significant implications for criminal investigation and integrated circuit design.

2. Results and Discussion

As photoluminescence guests, tetraphenylvinyl grafted bromophenylpyridine salt (TPE-BrN) or tetraphenylvinyl grafted phenylpyridine TPE-N derivatives were synthesized and characterized by ^{1}H NMR, ^{13}C NMR spectroscopies and high-resolution mass spectrometry (HRMS) (Figures S1–S6, Supporting Information). The melting points of TPE-BrN and TPE-N are 282°C

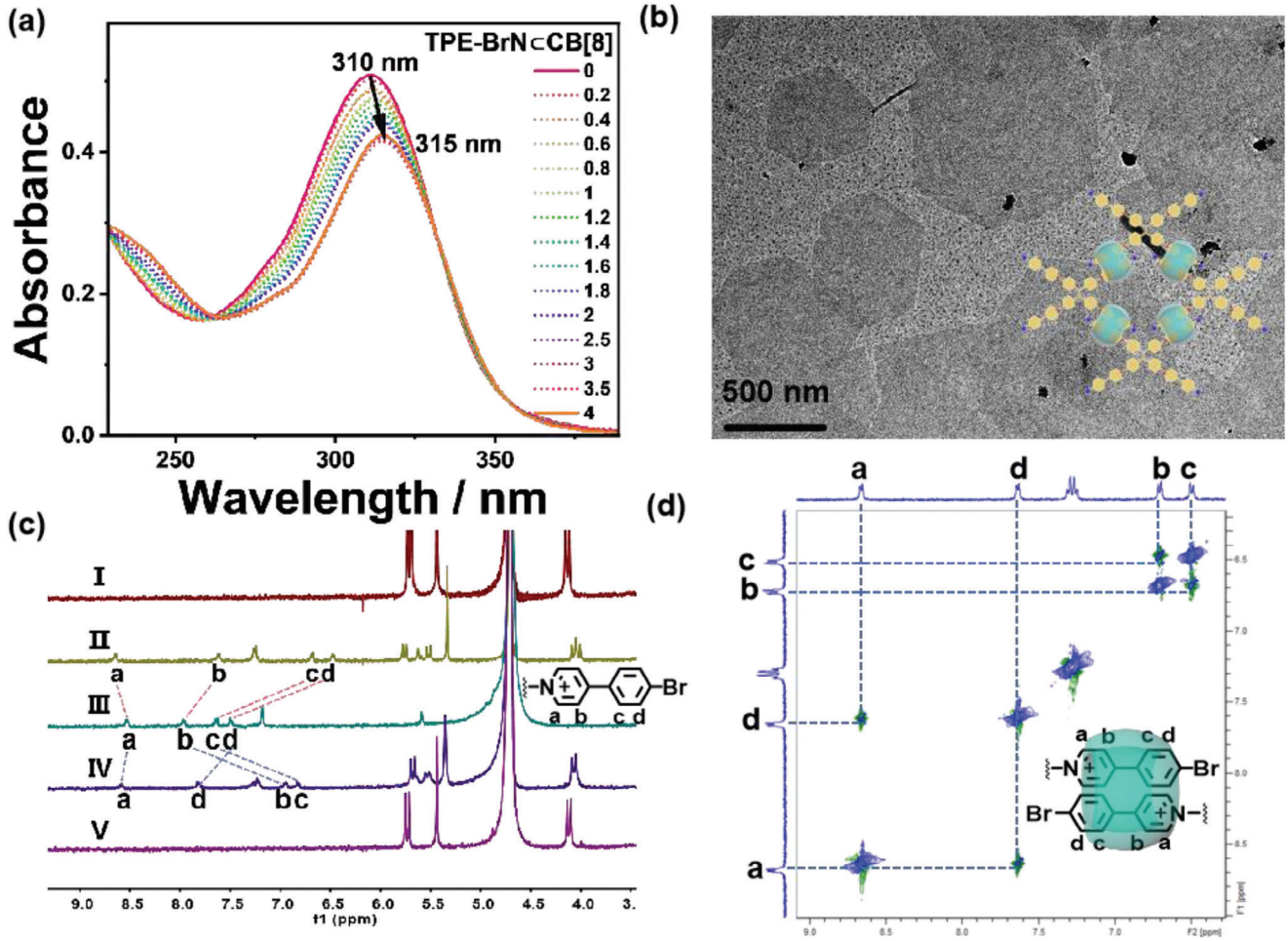

Figure 1. a) UV–vis absorption spectra of TPE-BrN in aqueous solution upon the gradual addition of CB[8] at 298 K ([TPE-BrN] = 1.0×10^{-5} M and [CB[8]] = 0–4.0×10^{-5} M). b) Transmission electronic microscopy image of TPE-BrN⊂CB[8] ([TPE-BrN] = 1.0×10^{-5} M and [CB[8]] = 2.0×10^{-5} M). c) ^{1}H NMR spectra (400 MHz, D_2O, 298 K) of (I) CB[7] ([CB[7]] = 1.0×10^{-4} M), (II) TPE-BrN⊂CB[7] ([TPE-BrN] = 1.0×10^{-4} M and [CB[7]] = 4.0×10^{-4} M), (III) TPE-BrN ([TPE-BrN] = 1.0×10^{-4} M), (IV) TPE-BrN⊂CB[8] ([TPE-BrN] = 1.0×10^{-4} M and [CB[8]] = 2.0×10^{-4} M) and (V) CB[8] ([CB[8]] = 1.0×10^{-4} M). d) ROESY spectrum (400 MHz, D_2O, 298 K) of TPE-BrN⊂CB[8] ([TPE-BrN] = 1.0×10^{-4} M and [CB[8]] = 2.0×10^{-4} M).

and 240°C, respectively. To study the cucurbituril confined photoluminescence performance,[29,30] we first carried out UV–vis spectroscopy experiments to investigate the binding behavior between TPE-BrN and cucurbituril in aqueous solution. The maximum absorption of TPE-BrN was shifted from 310 to 315 nm with the increase of CB[8] concentration (**Figure 1a**). Meanwhile, upon addition of CB[7], the absorption at 310 nm declined and shifted to 317 nm (Figure S11a, Supporting Information). Subsequently, the association constant between reference molecule 4-(4-bromophenyl)-1-ethylpyridin-1-ium (Br-N) and CB[8] was calculated to be 3.51×10^{12} M^{-2} based on the UV–vis absorption spectroscopic titration (Figure S12c, Supporting Information). And the association constant between reference molecule Br-N and CB[7] (Figure S12a, Supporting Information) was calculated to be 7.64×10^5 M^{-1} by using the same method. Then, the stoichiometric ratios of the host-guest inclusion complexes TPE-BrN:CB[7] and TPE-BrN:CB[8] were confirmed respectively to be 1:4 and 1:2 according to the corresponding Job's plot (Figure S11b,c, Supporting Information). Likewise, we measured the UV–vis titration spectra and Job's plot of TPE-N with CB[7] or CB[8]. Upon gradual addition of CB[7] from 0 to 6 equivalents, the absorption (Figure S24a, Supporting Information) at 300 nm decreased and the absorption at 300 shifted to 304 nm with the proportional addition of CB[8] (Figure 3a). The Job's experiments showed that the binding ratios of TPE-N to CB[7] and CB[8] were 1:4 and 1:2 in aqueous solution (Figure S25b,c, Supporting Information). Moreover, the fluorescence titration experiments of TPE-BrN (Figure S13b, Supporting Information) showed that the fluorescence emission at 375 nm attributed to the moiety of bromophenylpyridine salt decreased and a new peak appeared at 620 nm with the gradual addition of CB[8]. The fluorescence emission at 620 nm was assigned to TPE moiety, which may be due to the assembly limiting on TPE molecular vibration. The fluorescence intensity at 375 nm was enhanced with addition of CB[7] which was because that CB[7] could restrict bromophenylpyridinium molecular motion and improve its fluorescent emission at 375 nm (Figure S13a, Supporting Information). Besides, ^{1}H NMR titration experiments (Figures S15 and S16,

Supporting Information) were conducted to explore the binding behaviors of TPE-BrN⊂CB[7] and TPE-BrN⊂CB[8]. Furthermore, the signals of the protons (H_a, H_b, H_c, H_d) assigned to bromophenylpyridinium salt moiety shifted upon the addition of CB[7] (Figure 1d-II). The proton signals of $H_{b\text{-}d}$ underwent upfield shifts because of the shielding effect of CB[7], which suggested that the moiety bromophenylpyridinium salt was encapsulated into the cavity of CB[7]. At the same time, the H_a shifted downfield, proving that the proton was exposed to the edge of the CB[7] cavity. According to the comparison of the ^{1}H NMR spectroscopy between TPE-BrN and TPE-BrN⊂CB[8], we found that H_b and H_c moved towards upfield while the chemical shifts of H_a and H_d performed downfield shift (Figure 1d-IV) as a result of H_b and H_c being included by the cavity of CB[8]. 2D rotating-frame Overhauser effect spectroscopy (ROSEY) of TPE-BrN⊂CB[8] (Figure 1d) showed strong correlated signals between H_a and H_d as well as H_b and H_c, demonstrating that two bromophenylpyridinium units in the cavity of CB[8] formed the head-to-tail stacking mode, and $\pi-\pi$ stacking,[31] hydrophobic effect[32] and cation-dipole interaction synergistically contributed to the formation of TPE-BrN⊂CB[8] host-guest complex. Additionally, the diffusion-ordered NMR spectroscopy (DOSY) was conducted (Figure S18, Supporting Information), which showed the diffusion coefficient of TPE-BrN, TPE-BrN⊂CB[7] and TPE-BrN⊂CB[8] at 1.0×10^{-4} M were 1.866×10^{-10}, 1.344×10^{-10} and 1.391×10^{-10} m^2 s^{-1}. On the basis of the Stokes–Einstein relationship,[33] the larger the diffusion coefficient, the smaller the size of the supramolecular assemblies. It could be concluded that TPE-BrN⊂CB[8] and TPE-BrN⊂CB[7] complexes formed larger supramolecular assemblies compared with TPE-BrN. NMR experiment of TPE-N also proved a conclusion similar to TPE-BrN (Figures S27–S30, Supporting Information). The ^{1}H NMR titration experiment showed the signals of $H_{b\text{-}e}$ shfited to higher field, while H_a shfited to the lower field, indicating that $H_{b\text{-}e}$ were encapsulated into the cavity of CB[7] (Figure S27, Supporting Information). With the addition of CB[8], the ^{1}H NMR titration result showed a blunting of the peak attributed to phenylpyridinium part (Figure S28, Supporting Information). When CB[7] and CB[8] were added to more than 4 equivalents and 2 equivalents, respectively, neither of the ^{1}H NMR chemical shifts were changeable. These results were consistent with Job's experiments. To further study the morphology of the assemblies, transmission electron microscope (TEM), scanning electron microscopy (SEM), and dynamic light scattering (DLS) experiments were conducted (Figure 1b; Figures S19 and S21, Supporting Information). TPE-BrN presented nanofibers with microscale length, and it displayed homogenous nanoparticles with diameter of ≈ 180 nm after assembling with CB[7]. Specifically, the image of the TPE-BrN⊂CB[8] assembly exhibited 2D nanosheets. SEM image showed the similar results (Figure S19c,d, Supporting Information), which demonstrated that TPE-BrN performed nanofibers with length of several microns, and TPE-BrN⊂CB[7] was nanoparticles with a diameter of ≈ 180 nm. The data from DLS (Figure S20, Supporting Information) displayed that the TPE-BrN can aggregate upon the addition of CB[7] or CB[8], thereby further confirmed the aggregate trend identified by the techniques of TEM and SEM. Furthermore, TPE-BrN⊂CB[8] assembly was recorded by atomic force microscope (AFM), indicating the thickness of ≈4 nm, which may be due to the superposition of two layers of network (the height of a single CB[8] is 1.75 nm[34]). After reducing the concentration of TPE-BrN⊂CB[8], it could be observed that the formation of a single-layer network (Figure S21, Supporting Information). The topological morphology of TPE-N, TPE-N⊂CB[7], and TPE-N⊂CB[8] were also characterized, and there were some differences in dimensions according to the results of TEM and SEM (Figure S33, Supporting Information). TPE-N showed a maximum value of ≈ 5 μm nanofibers. And TPE-BrN⊂CB[7] exhibited nanoparticles with a diameter of ≈ 400 nm, while TPE-BrN⊂CB[8] displayed micron scale layered structure. In addition, the phosphorescence emission spectra of the TPE-BrN⊂CB[7] and TPE-BrN⊂CB[8] complexes in aqueous solution were measured, which showed weak emission peak at 510 nm (Figure S22a,b, Supporting Information). The time-resolved decay spectra fitted the lifetime of TPE-BrN⊂CB[7] at 510 nm and TPE-BrN⊂CB[8] at 510 nm, which were 18.80 and 11.32 μs (Figure S22c,d, Supporting Information). The above experiments suggested that various topological morphology supramolecular assemblies have been formed from TPE-BrN nanofibers to TPE-BrN⊂CB[7] nanoparticles and TPE-BrN⊂CB[8] nanosheets.

Considering the unique aggregation-Induced Emission (AIE) behavior of TPE groups and the excellent phosphorescence emission characteristics of bromophenylpyridine,[35,36] we investigated the photophysical properties of TPE-BrN@cucurbituril assemblies in the solid state. First, we prepared the TPE-BrN⊂CB[7] and TPE-BrN⊂CB[8] complexes in the solid state. When exposed to UV light at 365 nm, TPE-BrN showed very dim emission, and TPE-BrN⊂CB[7] emitted strong green emission, while TPE-BrN⊂CB[8] displayed bright yellow emission (**Figure 2a**). The photoluminescence spectra displayed that the emission peak of TPE-BrN (Figure S23a, Supporting Information) was centered at 470 nm, and TPE-BrN⊂CB[7] assembly showed significantly enhanced emission peak at 510 nm (Figure 2a). As for TPE-BrN⊂CB[8] assembly, the photoluminescence spectrum revealed a red-shift to 560 nm (Figure 2a). The 2D assembly TPE-BrN⊂CB[8] enhanced restriction on TPE molecular vibration, thereby inducing a red shift in solid-state photoluminescence emission from 470 to 560 nm. The fluorescence lifetime of TPE-BrN⊂CB[7] at 510 nm and TPE-BrN⊂CB[8] at 560 nm were 4.02 and 3.84 ns (Figure 2c). The photoluminescent quantum yield values of TPE-BrN, TPE-BrN⊂CB[7] and TPE-BrN⊂CB[8] were calculated as 12.60%, 24.70% and 13.74% (Figure S24, Supporting Information). Furthermore, we investigated the phosphorescence emission properties for TPE-BrN in the solid state. The phosphorescence emission spectra (delay 0.050 ms) of TPE-BrN⊂CB[6] (Figure S23c, Supporting Information) and TPE-BrN⊂CB[7] (Figure 2b) showed an emission peak at around 510 nm. The phosphorescence emission of TPE-BrN⊂CB[8] also revealed an emission peak at 510 nm (Figure 2b). The explanation for these properties was that the cavity of the cucurbituril limited the molecular vibration of the BrN portion and greatly weakened non-radiative transitions, inducing the appearance of effective phosphorescence emission.[37,38] Excitedly, the phosphorescence intensity of TPE-BrN⊂CB[6] was about fivefold stronger than TPE-BrN⊂CB[7], and nearly tenfold stronger than TPE-BrN⊂CB[8], which related to the size of the cucurbituril cavity. And the time-resolved decay curves of these complexes were measured, which showed the phosphorescence lifetime of

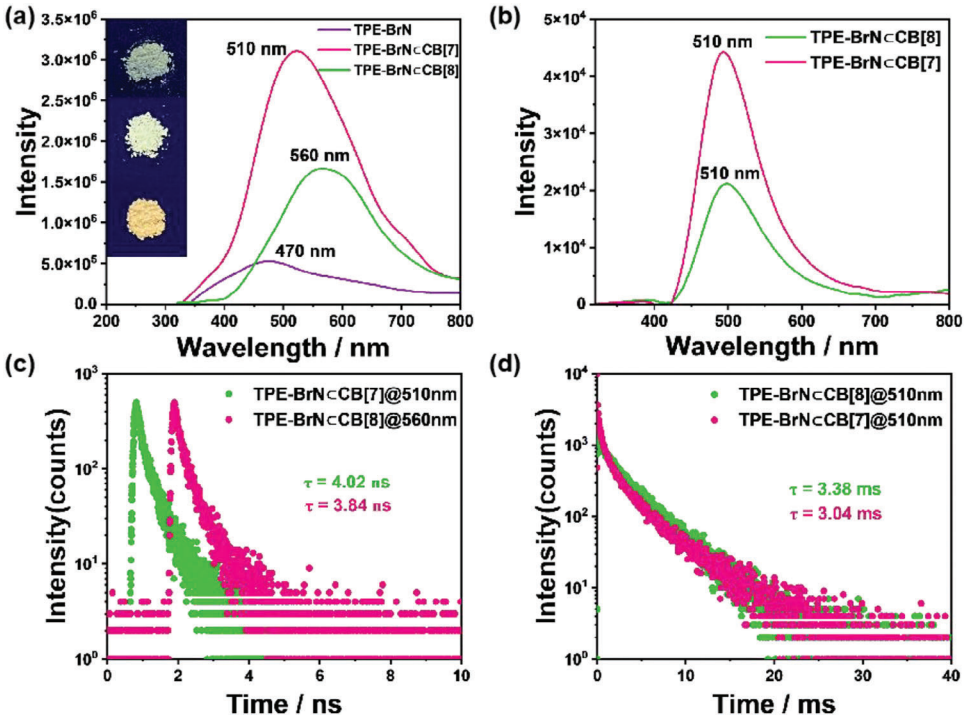

Figure 2. a) The photoluminescence emission spectra of TPE-BrN, TPE-BrN⊂CB[7], and TPE-BrN⊂CB[8] in the solid state at 298 K (λ_{ex} = 310 nm). Inset: Photograph from top to bottom of the solid TPE-BrN, TPE-BrN⊂CB[7], and TPE-BrN⊂CB[8] upon irradiation with 365 nm UV. b) The phosphorescence emission spectra (delayed 0.050 ms) of TPE-BrN⊂CB[7] and TPE-BrN⊂CB[8] in the solid state at 298 K (λ_{ex} = 310 nm). c) The fluorescence lifetime decay curves of TPE-BrN⊂CB[7] at 510 nm and TPE-BrN⊂CB[8] at 560 nm in the solid state at 298 K. d) The phosphorescence lifetime decay curves of TPE-BrN⊂CB[7] and TPE-BrN⊂CB[8] at 510 nm in the solid state at 298 K.

TPE-BrN⊂CB[6] (Figure S23d, Supporting Information), TPE-BrN⊂CB[7] (Figure 2d) and TPE-BrN⊂CB[8] (Figure 2d) were 8.28, 3.04 and 3.38 ms, respectively.

Furthermore, we studied the photophysical properties of TPE-N assemblies. As illustrated in **Figure 3b**, it could be seen that TPE-N⊂CB[7] emitted green light and TPE-N⊂CB[8] emitted yellow light with the excitation of 365 nm UV light, while individual TPE-N emitted dark yellow light. The fluorescence emission wavelength of TPE-N and TPE-N⊂CB[7] were at 470 and 510 nm (Figure 3b). The fluorescence emission of TPE-N⊂CB[8] (Figure 3b) was centered at 560 nm in the solid state, which was assigned to the AIE behavior of TPE moiety. The redshift of fluorescence emission for TPE-BrN⊂CB[8] from 470 to 560 nm was attributed to the charge transfer process caused by supramolecular conjugation enhancement. The photoluminescence quantum yield of TPE-N⊂CB[6], TPE-N⊂CB[7] and TPE-N⊂CB[8] were 3.52%, 3.21% and 1.79% (Figure S32, Supporting Information). Additionally, we measured their phosphorescence emission spectra (delayed 0.050 ms), which displayed the dominant emission peak at 470 nm for TPE-N⊂CB[6], 510 nm for TPE-N⊂CB[7], and 530 nm TPE-N⊂CB[8], respectively (Figure 3c; Figure S31c, Supporting Information). The phosphorescence lifetime was 0.808 s for TPE-N⊂CB[6] at 470 nm (Figure S31d, Supporting Information), 0.965 ms for TPE-N⊂CB[7] at 510 nm, and 1.202 ms for TPE-N⊂CB[8] at 530 nm (Figure 3d). The different lifetimes of host-guest complexes were mainly attribute to (1) CB[6] can encapsulate the guests to form tight 4:1 host-guest complexes, resulting in the long lifetime (0.808 s), (2) although the CB[7] encapsulate the guests to form 4:1 host-guest complexes, the cavity size was larger than that of CB[6], leading to the loose encapsulation with short lifetime (0.965 ms), (3) the CB[8] encapsulate the guests to form 2:1 host-guest complexes with slight short lifetime (1.202 ms). Above results jointly demonstrated the uncommon photophysical behavior for TPE-N assemblies in AIE emission and phosphorescence emission.

In the light of the excellent multidimensional topological morphology and phosphorescence emission properties of the TPE-BrN solid complexes, we explored the potential as the energy donor for the TS-FRET process.[39] TS-FRET process has attracted widespread attention due to the ability to construct long-lived luminescent materials,[40,41] which takes place from the triplet-state of donors to the singlet-state of organic dyes. We selected the organic dye Nile red (NiR) as the acceptor. NiR is environmentally selective and has almost no fluorescence in aqueous solution. On the contrary, it is intensely fluorescent in hydrophobic environments. Tetracation guest TPE-BrN and CB[8] could form a 2:1 host-guest complex, which allowed TPE-BrN⊂CB[8] to self-assemble into a 2D network structure in solution (Figure S35, Supporting Information). Owing to the hydrophobic interaction, NiR dyes can be doped into the pores of the 2D network, creating necessary conditions for the short distance between the donor and acceptor required for TS-FRET. The absorption band of NiR overlaps with the emission band of TPE-BrN⊂CB[8] to a certain extent (**Figure 4b**). As depicted in Figure 4c, with the stepwise addition of NiR, the phosphorescence emission (delayed 0.050 ms) peak at 510 nm gradually decreased and a new peak

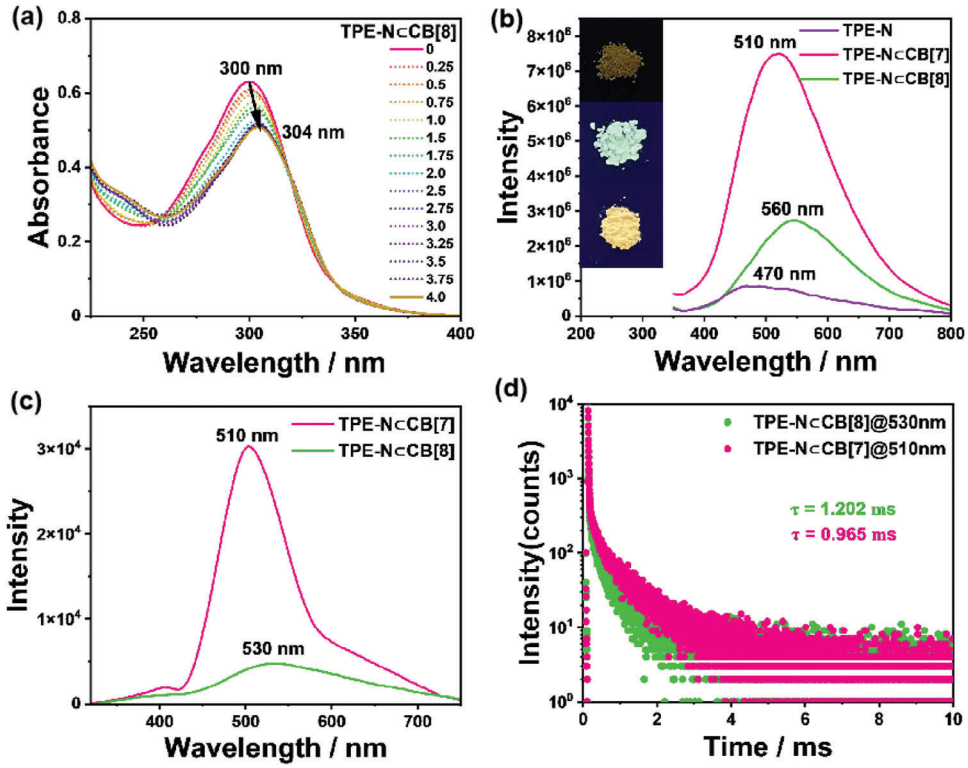

Figure 3. a) UV–vis absorption spectra of TPE-N in aqueous solution upon the gradual addition of CB[8] at 298 K ([TPE-N] = 1.0×10^{-5} M and [CB[8]] = 0–4.0×10^{-5} M). b) The fluorescence emission spectra of TPE-N, TPE-N⊂CB[7], and TPE-N⊂CB[8] in the solid state at 298 K (λ_{ex} = 300 nm). Inset: Photograph from top to bottom of the solid TPE-N, TPE-N⊂CB[7], and TPE-N⊂CB[8] upon irradiation with 365 nm UV. c) The phosphorescence emission spectra (delayed 0.050 ms) of TPE-N⊂CB[7] and TPE-N⊂CB[8] in the solid state at 298 K (λ_{ex} = 300 nm). d) The phosphorescence lifetime decay curve of TPE-N⊂CB[7] at 510 nm and TPE-N⊂CB[8] at 530 nm in the solid state at 298 K.

appeared at 675 nm, indicating the occurrence of TS-FRET from TPE-BrN⊂CB[8] to NiR. The emission would no longer change when adding content of NiR reached up to 4%. In control experiments (Figure S34, Supporting Information), there was no long-lived emission peak at 675 nm when using the optimal excitation of NiR (550 nm), which indicated the variation of the phosphorescence was attributed to the energy transfer from TPE-BrN⊂CB[8] to NiR. Then the time-resolved decay spectra recorded the lifetimes at 510 and 675 nm. The lifetime at 510 nm reduced from 3.38 ms to 558.86 µs and the lifetime at 675 nm was 554.28 µs, which revealed that there was indeed a new long-lived peak at 675 nm. The phenomenon demonstrated that the energy transferred from the triplet state of TPE-BrN⊂CB[8] to the singlet state of NiR. The energy transfer efficiency (Φ_{ET})[18] was calculated to be as high as 99%, the AE (antenna effect) was calculated as 153 at a acceptor doping ratio of 4% (Figure S34, Supporting Information). These experiments suggested that the 2D network formed by TPE-BrN and CB[8] has the ability to dope fluorescent dyes, which reduced the distance between the donor TPE-BrN⊂CB[8] and the acceptor NiR to ensure the occurrence of TS-FRET. Subsequently, the photoluminescence emission spectra were measured, which exhibited that the new peaks at 675 nm emerged and the emission peak located at 560 nm decreased indicating the Förster resonance energy transfer process[42–44] from the singlet-state of TPE to the singlet-state of NiR within the 2D network (Figure S36a, Supporting Information). As elucidated in the Figure 4d, the CIE diagram showed that it moved from blue emission region to the red region. Therefore, the color transformation of luminescent materials can be achieved via energy transfer process. As the control experiments, we also measured the phosphorescence spectra of TPE-BrN⊂CB[6] and TPE-BrN⊂CB[7] after doping with NiR (Figure S36b,c, Supporting Information). To be specific, as the proportion of NiR addition increased, the phosphorescence emission (delay 0.050 ms) peak at 510 nm gradually decreased, but the emission of both systems at 675 nm was invisible. These phenomena declared that after the addition of NiR, TPE-BrN⊂CB[6] and TPE-BrN⊂CB[7] could not undergo an effective TS-FRET process. These results happened to account for the ability of TPE-BrN⊂CB[8] to form the 2D network structure to dope organic dye for efficient TS-FRET process or SS-FRET process.

Given the excellent luminescent behavior and energy transfer effect of TPE-BrN⊂CB[8] supramolecular assemblies, we have conducted some experiments to expand the application of these materials. At crime scenes, fingerprints are often the key to solving crimes. The imprint left by latent human fingerprints consists of sweat and sebum, which can absorb powder. Therefore, TPE-BrN⊂CB[8]@NiR was competent to collect fingerprints due to its excellent color rendering effect. We mixed montmorillonite (MMT) in the prepared material in order to improve the adsorption of the powder in the fingerprint area.[45] First, the imaging effect on the glass was tested. Under 365 nm

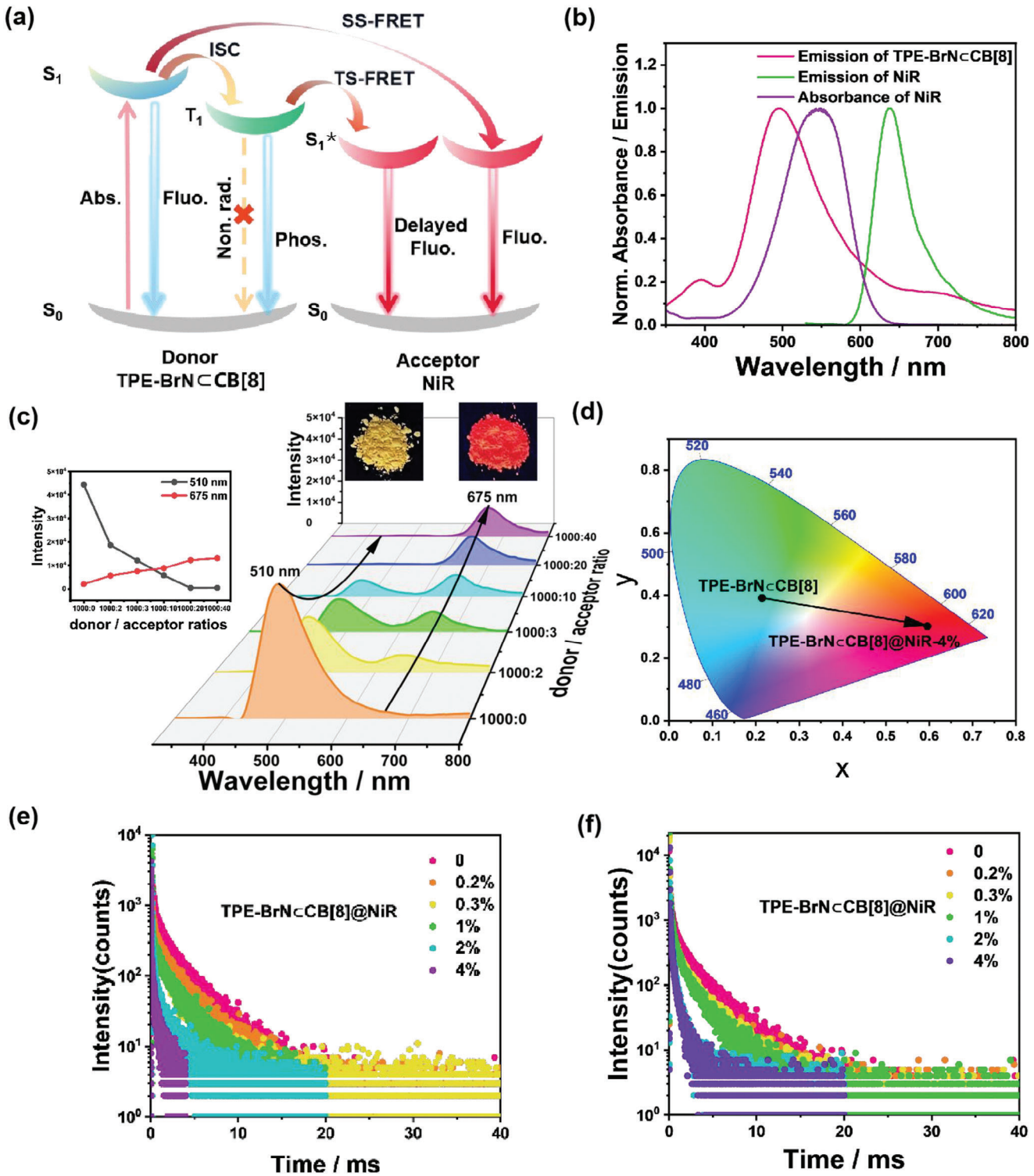

Figure 4. a) Diagram of the possible mechanism for the supramolecular energy transfer process. b) Normalized phosphorescence emission spectrum of TPE-BrN⊂CB[8], and the absorption and emission spectra of NiR. c) Phosphorescence emission spectra (delayed 0.050 ms) of TPE-BrN⊂CB[8] with increasing the doping concentration of NiR. d) CIE 1931 chromaticity diagram of TPE-BrN⊂CB[8] and TPE-BrN⊂CB[8]@NiR-4%. The time-resolved intensity decay curves of TPE-BrN⊂CB[8] with increasing the doping concentration of NiR were measured at e) 510 and f) at 675 nm, respectively.

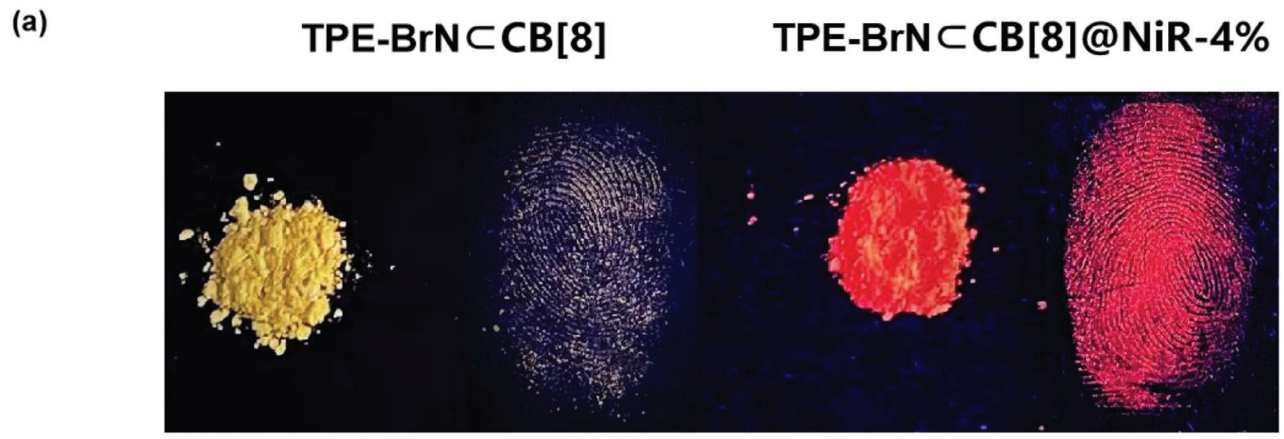

(b)

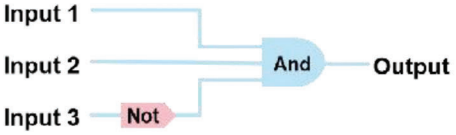

Input 1	Input 2	Input 3	Output
TPE-BrN	CB[8]	NiR	FL 560nm
0	0	0	0
1	0	0	0
0	1	0	0
0	0	1	0
1	1	0	1
1	0	1	0
0	1	1	0
1	1	1	0

(c)

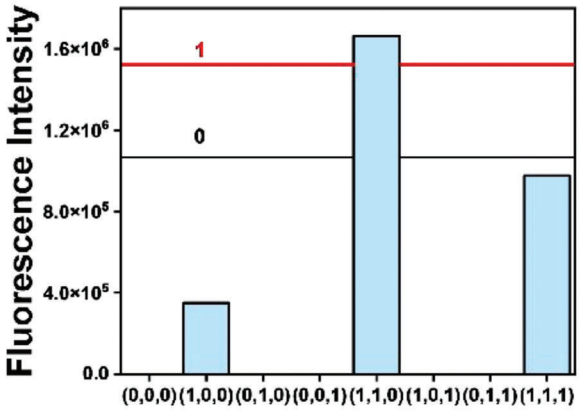

(d)

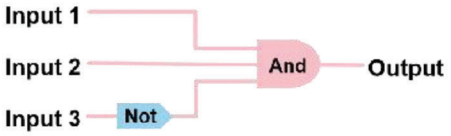

Input 1	Input 2	Input 3	Output
TPE-BrN	CB[8]	NiR	Pho 510nm
0	0	0	0
1	0	0	0
0	1	0	0
0	0	1	0
1	1	0	1
1	0	1	0
0	1	1	0
1	1	1	0

(e)

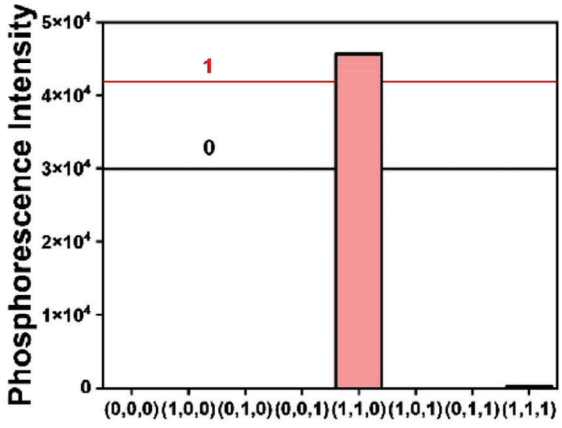

Figure 5. a) Photographs and fingerprint imagings of TPE-BrN⊂CB[8] and TPE-BrN⊂CB[8]@NiR-4% under 365 nm UV light. b,d) Two logic gates and c, e) corresponding truth tables in different situations. The output is set to the intensity of fluorescence at 560 nm and phosphorescence at 510 nm (λ_{ex} = 310 nm).

UV light, TPE-BrN⊂CB[8]@NiR can be observed to emit a bright red fluorescent fingerprint pattern (**Figure 5a**). In contrast, TPE-BrN⊂CB[8]-MMT showed poor imaging (Figure 5a), while MMT, TPE-BrN-MMT, and NiR-MMT could not be detected for imaging. Subsequently, we also have successfully applied these materials to construct many logic gate systems. The AND logic gate system has multiple inputs but only one output. The NOT logic gate means that the output is 0 when input 1, and 1 when input 0. As shown in Figure 5b,d, we take the different components of the assembly as inputs and the fluorescence emission at 560 nm or the phosphorescence emission at 510 nm or the phosphorescence emission at 675 nm as output. As displayed in Figure 5c,e, we defined different intensity intervals as 0 or 1. Thereby, we designed two kinds of logic gate systems with fluorescence and phosphorescence output. The input of current logic circuits represents different types of supramolecular assemblies. When only TPE-BrN and CB[8] coexist, the two logic gate systems can output true values. As the composition of inputs changes, the output information also becomes more complex accordingly, which provides new ideas for the application of integrated circuits.

3. Conclusion

In summary, we have successfully constructed a TS-FRET system with a solid-state supramolecular 2D network structure based on the host-guest interaction of TPE-BrN and CB[8]. CB[8] could not only induce efficient fluorescence-phosphorescence dual emission of TPE-BrN at 560 and 510 nm, but also contribute to the topological transformation from nanofiber to 2D network structure. Benefiting from the ordered structure, organic dye (NiR) could dope with a trace amount into the 2D framework to achieve highly efficient TS-FRET process and SS-FRET process. Interestingly, these effective NIR long-lived photo luminescent materials were utilized for imaging of fingerprints and logic gates, which suggested that the current study could provide a new approach for activating TS-FRET based on macrocyclic confinement supramolecular 2D organic framework.

4. Experimental Section

Instrumentation: All reagents and solvents were obtained from commercial suppliers and were used as supplied, unless otherwise noted. NMR spectra were recorded on an Ascend 400 MHz instrument. ROESY and DOSY spectra were measured on a zhongke-Oxford I-400 instrument. High-resolution MS was performed on a Fouier transform ion cyclotron resonance mass spertrometer in electrospray ionization mode. UV-vis absorption spectra were recorded on a Shimadzu UV-3600 spectrophotometer with a PTC-348WI temperature controller in a quartz cell (light path 10 mm) at 298 K. Fluorescence spectra were measured in a conventional rectangular quartz cell (10 × 10 × 45 mm) on a Varian CARY Eclipse Fluorescence Spectrophotometer equipped with a constant temperature water bath. Photoluminescence spectra, lifetime, and quantum yield were obtained on a Spectrofluorometer FS5 instrument (Edinburg Instruments, Livingstone, UK). The photoluminescence spectra for each data point was delayed 0.050 ms to ensure that the first 0.050 ms were not collected to eliminate the fluorescence emission. TEM experiments were carried out on a FEI Tecnai G2 F20 microscope operating at 200 KV. Scanning electron microscopy images were obtained with a FE-SEM (Apreo S LoVac) scanning electron microscope. AFM images were recorded on Dimension Icon microscope (Bruker). Dynamic Light Scattering (DLS) was examined by using a laser lights-scattering spectrometer (BI-200SM) equipped with a digital correlator (Turbo Corr) at 636 nm at a scattering angle of 90°.

Materials and Methods: Respectively, 5 mmol TPE-BrN and 20 mmol CB[6], 5 mmol TPE-BrN and 20 mmol CB[7], 5 mmol TPE-BrN and 10 mmol CB[8] were added to the agate mortar. After adding one drop of deionized water, thoroughly ground them and freeze dried to obtain anhydrous solid-state samples. 5 mmol TPE-BrN⊂CB[8] and 2 mg of montmorillonite were added into the agate mortar for thorough grinding to obtain the material. The same method for the logic gates experiments.

The volunteers who provided fingerprints participated in the study with informed consent and were allowed to publish these images. The volunteers gently wiped their foreheads with their index fingers and then pressed their fingers on the surface of glass to obtain fingerprints. Next, the powder material above the fingerprint area was covered, and blew away the excess powder. The fingerprint images were photographed using a mobile phone under 365 nm UV light.

Calculation of Quantum Yield: The solid quantum yield was measured by the Quantum Integrating Sphere method on Spectrofluorometer FS5. Specifically, the fluorescence (phosphorescence) quantum yield was calculated by measuring the fluorescence (phosphorescence) emission and absorption of the test sample and blank sample. The calculation formula was $QY_X = QY_{ST} \times (Grad_X/Grad_{ST}) \times (\eta_X^2/\eta_{ST}^2)$, where ST and X represent the standard group and experimental group, respectively; QY is the fluorescence (phosphorescence) quantum yield; Grad is the ratio of fluorescence (phosphorescence) intensity to absorbance. In the test, the η_X and η_{ST} was 1, respectively.

Supporting Information

Supporting Information is available from the Wiley Online Library or from the author.

Acknowledgements

This work was financially supported by the National Natural Science Foundation of China (grant nos. 22131008). F.-F.L. and M.H. contributed equally to this work. Y. L. acquired the funding, revised the manuscript, and supervised the project.

Conflict of Interest

The authors declare no conflict of interest.

Data Availability Statement

The data that support the findings of this study are available in the supplementary material of this article.

Keywords

2D network, cucurbituril confinement, NIR delayed emission, room-temperature phosphorescence, triplet-state to singlet-state Förster resonance energy transfer

Received: February 17, 2024
Revised: April 5, 2024
Published online:

[1] Y. Wang, H. Gao, J. Yang, M. Fang, D. Ding, B. Z. Tang, Z. Li, *Adv. Mater.* **2021**, *33*, 2007811.

[2] X.-F. Wang, H. Xiao, P.-Z. Chen, Q.-Z. Yang, B. Chen, C.-H. Tung, Y.-Z. Chen, L.-Z. Wu, *J. Am. Chem. Soc.* **2019**, *141*, 5045.
[3] X. Y. Dai, M. Huo, X. Dong, Y. Y. Hu, Y. Liu, *Adv. Mater.* **2022**, *34*, 2203534.
[4] J. Zhang, B. He, Y. Hu, P. Alam, H. Zhang, J. W. Y. Lam, B. Z. Tang, *Adv. Mater.* **2021**, *33*, 2008071.
[5] J. Song, L. Ma, S. Sun, H. Tian, X. Ma, *Angew. Chem. Int. Ed.* **2022**, *61*, e202206157.
[6] H. Li, H. Li, W. Wang, Y. Tao, S. Wang, Q. Yang, Y. Jiang, C. Zheng, W. Huang, R. Chen, *Angew. Chem. Int. Ed.* **2020**, *59*, 4756.
[7] Z. Zong, Q. Zhang, S. H. Qiu, Q. Wang, C. Zhao, C. X. Zhao, H. Tian, D. H. Qu, *Angew. Chem. Int. Ed.* **2022**, *61*, e202116414.
[8] Q. Wang, B. Lin, M. Chen, C. Zhao, H. Tian, D.-H. Qu, *Nat. Commun.* **2022**, *13*, 4185.
[9] H. Y. Zhou, D. W. Zhang, M. Li, C. F. Chen, *Angew. Chem. Int. Ed.* **2022**, *61*, e202117872.
[10] X. Ma, J. Wang, H. Tian, *Acc. Chem. Res.* **2019**, *52*, 738.
[11] X. Y. Dai, M. Huo, Y. Liu, *Nat. Rev. Chem.* **2023**, *7*, 854.
[12] B. Chen, W. Huang, X. Nie, F. Liao, H. Miao, X. Zhang, G. Zhang, *Angew. Chem., Int. Ed.* **2021**, *60*, 16970.
[13] C. Wang, Y. H. Liu, Y. Liu, *Small* **2022**, *18*, 2201821.
[14] Y. Y. Hu, X. Y. Dai, X. Dong, M. Huo, Y. Liu, *Angew. Chem., Int. Ed.* **2022**, *61*, e202213097.
[15] N. Gan, H. Shi, Z. An, W. Huang, *Adv. Funct. Mater.* **2018**, *28*, 1802657.
[16] B. Zhou, D. Yan, *Adv. Funct. Mater.* **2019**, *29*, 1807599.
[17] S. Garain, B. C. Garain, M. Eswaramoorthy, S. K. Pati, S. J. George, *Angew. Chem. Int. Ed.* **2021**, *60*, 19720.
[18] M. Huo, X. Y. Dai, Y. Liu, *Small* **2022**, *18*, 2104514.
[19] J. Yu, H. Wang, Y. Liu, *Adv. Opt. Mater.* **2022**, *10*, 2201761.
[20] S.-P. Jin, H.-L. Wu, L.-P. Zhang, G.-Y. Yang, B. Yang, *Mater. Chem. Front.* **2023**, *7*, 1354.
[21] G. Zhou, M. Li, J. Zhao, M. S. Molokeev, Z. Xia, *Adv. Opt. Mater.* **2019**, *7*, 1901335.
[22] H. Zheng, Z. Zhao, J. B. Phan, H. Ning, Q. Huang, R. Wang, J. Zhang, W. Chen, *ACS Appl. Mater. Interfaces* **2020**, *12*, 2145.
[23] Y. Yang, X. Yang, X. Fang, K. Z. Wang, D. Yan, *Adv. Sci.* **2018**, *5*, 1801187.
[24] X. Wu, M. Liu, J. Niu, Q. Liu, X. Jiang, Y. Zheng, Y. Qian, Y.-M. Zhang, J. Shen, Y. Liu, *Chem. Sci.* **2023**, *14*, 1724.
[25] J. Yu, J. Niu, J. Yue, L.-H. Wang, Y. Liu, *ACS Nano* **2023**, *17*, 19349.
[26] K.-D. Zhang, J. Tian, D. Hanifi, Y. Zhang, A. C.-H. Sue, T.-Y. Zhou, L. Zhang, X. Zhao, Y. Liu, Z.-T. Li, *J. Am. Chem. Soc.* **2013**, *135*, 17913.
[27] Y. Li, Y. Dong, X. Miao, Y. Ren, B. Zhang, P. Wang, Y. Yu, B. Li, L. Isaacs, L. Cao, *Angew. Chem. Int. Ed.* **2018**, *57*, 729.
[28] Y. Li, Q. Li, X. Miao, C. Qin, D. Chu, L. Cao, *Angew. Chem. Int. Ed.* **2021**, *60*, 6744.
[29] W.-L. Zhou, W. Lin, Y. Chen, X.-Y. Dai, Z. Liu, Y. Liu, *Chem. Sci.* **2022**, *13*, 573.
[30] F. F. Shen, Z. Liu, H. J. Yu, H. Wang, X. Xu, Y. Liu, *Adv. Opt. Mater.* **2022**, *10*, 2200245.
[31] W. Liu, J. Wang, Y. Gong, Q. Liao, Q. Dang, Z. Li, Z. Bo, *Angew. Chem. Int. Ed.* **2020**, *59*, 20161.
[32] X.-Q. Liu, K. Zhang, J.-F. Gao, Y.-Z. Chen, C.-H. Tung, L.-Z. Wu, *Angew. Chem. Int. Ed.* **2020**, *59*, 23456.
[33] W. W. Xing, H. J. Wang, Z. Liu, Z. Yu, H.-Y. Zhang, Y. Liu, *Adv. Opt. Mater.* **2023**, *11*, 2202588.
[34] K. Kim, N. Selvapalam, Y. H. Ko, K. M. Park, D. Kim, J. Kim, *Chem. Soc. Rev.* **2007**, *36*, 267.
[35] Z.-Y. Zhang, Y. Liu, *Chem. Sci.* **2019**, *10*, 7773.
[36] Z. Y. Zhang, Y. Chen, Y. Liu, *Angew. Chem. Int. Ed.* **2019**, *58*, 6028.
[37] A. Cheng, H. Su, X. Gu, W. Zhang, B. Zhang, M. Zhou, J. Jiang, X. Zhang, G. Zhang, *Angew. Chem., Int. Ed.* **2023**, *62*, e202312627.
[38] H. Wu, L. Gu, G. V. Baryshnikov, H. Wang, B. F. Minaev, H. Ågren, Y. Zhao, *ACS Appl. Mater. Interfaces* **2020**, *12*, 20765.
[39] S. Kuila, S. J. George, *Angew. Chem. Int. Ed.* **2020**, *59*, 9393.
[40] A. Cheng, Y. Jiang, H. Su, B. Zhang, J. Jiang, T. Wang, Y. Luo, G. Zhang, *Angew. Chem. Int. Ed.* **2022**, *61*, e202206366.
[41] J. Guo, C. Yang, Y. Zhao, *Acc. Chem. Res.* **2022**, *55*, 1160.
[42] M. Tian, Z. Wang, X. Yuan, H. Zhang, Z. Liu, Y. Liu, *Adv. Funct. Mater.* **2023**, *33*, 2300779.
[43] R. Zhang, Y. Chen, L. Chen, Y. Zhang, Y. Liu, *Adv. Optical. Mater.* **2023**, *11*, 2300101.
[44] D. V. Berdnikova, E. Y. Chernikova, *ChemPhotoChem* **2024**, *8*, 202300140.
[45] T. Xiao, L. Zhang, D. Chen, Q. Zhang, Q. Wang, Z.-Y. Li, X.-Q. Sun, *Org. Chem. Front.* **2023**, *10*, 3245.